Cent. Eur. J. Phys. • 9(2) • 2011 • 519-529
DOI: 10.2478/s11534-010-0086-9

VERSITA

Central European Journal of **Physics**

Resistance simulations for junctions of SW and MW carbon nanotubes with various metal substrates*

Research Article

Yuri N. Shunin[1,2†], Yuri F. Zhukovskii[2‡], Natalia Burlutskaya[1§], Stefano Bellucci[3¶]

1 *Information Systems Management Institute, Riga, Latvia*

2 *Institute of Solid State Physics, University of Latvia, Riga, Latvia*

3 *INFN-Laboratori Nazionali di Frascati, Via Enrico Fermi 40, Frascati, Italy*

Received 19 June 2010; accepted 11 September 2010

Abstract: This theoretical study focuses on junctions between the carbon nanotubes (CNTs) and contacting metallic elements of a nanocircuit. Numerical simulations on the conductance and resistance of these contacts have been performed using the multiple scattering theory and the effective media cluster approach. Two models for CNT-metal contacts have been considered in this paper: a) first principles "liquid metal" model and b) semi-empirical model of "effective bonds" based on Landauer notions on ballistic conductivity. Within the latter, which is a more adequate description of chirality effects, we have simulated both single-wall (SW) and multi-wall (MW) CNTs with different morphology. Results of calculations on resistance for different CNT-Me contacts look quantitatively realistic (from several to hundreds kOhm, depending on chirality, diameter and thickness of MW CNT). The inter-wall transparency coefficient for MW CNT has been also simulated, as an indicator of possible 'radial current' losses.

PACS (2008): 63.22.Gh, 71.10.Ca, 71.15.Ap, 73.63.Fg, 73.63.Rt, 85.35.Kt

Keywords: Carbon nanotubes • SW and MW morphology • junction between the CNT and metal substrate • scattering theory • electronic structure calculations • resistance of CNT-Me contact • inter-wall transparency in MW CNTs

1. Introduction

In order to overcome disadvantages of contemporary microtechnology, the miniaturization of electronic devices, a high integration level and the increase of the operation frequencies and power density are required, including the use of adequate materials and innovative chip interconnects. Due to their unique physical properties, carbon nanotubes (CNTs) attract permanently growing techno-

*presented at the 6th International Conference on Functional Materials and Nanotechnologies, March 17-19, 2010, Riga, Latvia.

†E-mail: shunin@isma.lv (Corresponding author)
‡E-mail: quantzh@latnet.lv
§E-mail: natalja.burlucka@isma.lv
¶E-mail: Stefano.Bellucci@lnf.infn.it

logical interest, for example, as promising candidates for nano-interconnects in a high-speed electronics [1]. The main aim of the current study is the implementation of advanced simulation models for a proper description of the electrical resistance for contacts between carbon nanotubes of different morphology and metallic substrates of different nature. An adequate description of CNT chirality is one of the key points for proper simulations on electric properties of CNT-based nanoelectronic devices. The single-wall carbon nanotube can be constructed by wrapping up the graphene monolayer in such a way that the two equivalent sites of the hexagonal lattice coincide. The wrapping vector **C**, which defines the relative location of the two sites, is specified by a pair of integers (n, m) that decompose **C** to the two unit vectors $\mathbf{a}_1$ and $\mathbf{a}_2$ (*i.e.*, $\mathbf{C} = n\mathbf{a}_1 + m\mathbf{a}_2$). The nanotube is called 'armchair' if n equals m, whereas if $m = 0$ such a CNT possesses 'zigzag' chirality. All the other nanotubes belong to the 'chiral' type and have a finite wrapping angle $\phi : 0° < \phi < 30°$ [2].

The resistance of contacts between CNTs and metallic catalytic substrates can considerably exceed that observed in the separate parts of these junctions [3]. The conductance between real metals and CNTs still occurs, however, mainly due to the scattering processes, which are estimated to be rather weak [4]. Fig. 1 represents the contacts between a CNT and metallic electrodes, as a prototype nanodevice. This is a main subject of our current research and modeling. The toroidal region (CNT-Me) is the object of a microscopic approach responsible for the main contribution to the resistance. As to the nanotube itself and the metallic substrate, their resistances may be considered as macroscopic parameters.

The electronic structure for the CNT-Me interconnect can be evaluated through the electronic density of states (DOS) for carbon-metal contact considered as a 'disordered alloy', where clusters containing both C and Me atoms behave as scattering centers. The computational procedure developed by us for these calculations [5] is based on the construction of cluster potentials and the evaluation of both scattering (S) and transfer (T) matrices.

The general model of multiple scattering with effective media approximation (EMA) for condensed matter based on the approach of atomic cluster is presented in Fig. 2. The cluster formalism was successfully applied for metallic Cu [5], as well as for both elemental (Ge and Si) and binary (As_xSe_{1-x} and Sb_xSe_{1-x}) semiconductors [6]. A special attention was paid for the latter, since in solid solutions the concept of statistical weighing was applied for the binary components [5, 6]. When using the coherent potential approximation (CPA) as EMA approximation, the

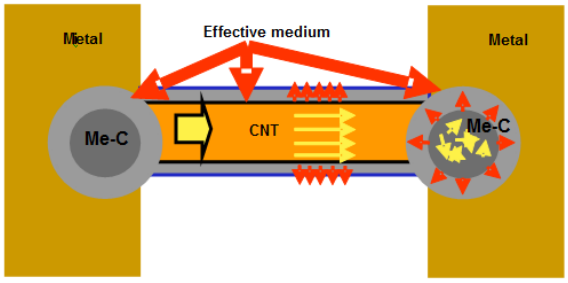

Figure 1. Model of CNT-Me interconnect as a prototype of nanodevice.

resistance of the interconnect can be evaluated through the Kubo-Greenwood formalism [7] and Ziman model [8]. Both Figs. 3 and 4 depict the idealized images of contacts between CNTs and the Ni substrate.

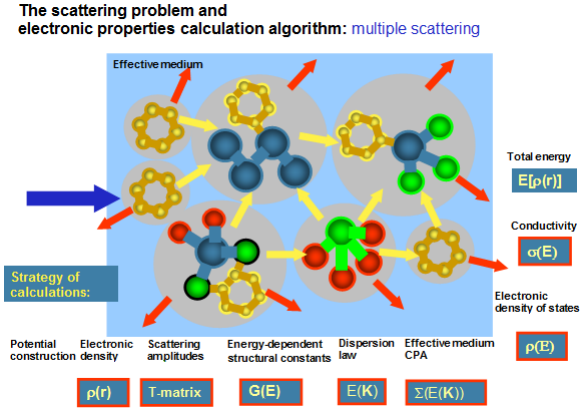

Figure 2. Multiple scattering problem for the system of clusters as multiple scattering model of condensed matter: strategy of calculations of fundamental properties of condensed medium described within the effective media approximation.

The electronic structure of the CNT-Ni interconnects, in the simplest case, can be evaluated through the DOS for C-Ni contact, considered as a 'disordered alloy', where clusters containing carbon and nickel atoms are the scattering centers. However, in many cases, we have to develop more complicated structural models for CNT-metal junctions, based on their precise atomistic structures, which take into account the CNT chirality effect. This is also the subject of the current study. When estimating the resistance of a junction between the nanotube and the substrate, the main problem is caused by the influence of the nanotube chirality on the resistance of SW and MW CNT-Me interconnects (Me = Ni, Cu, Ag, Pd, Pt, Au), for

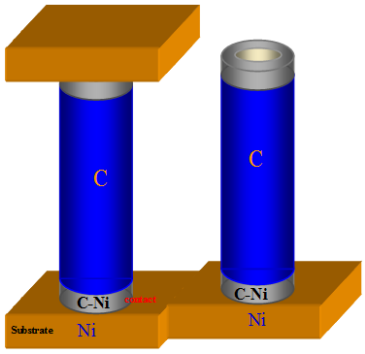

Figure 3. Fragment of interconnects between the Ni substrate and C nanotubes.

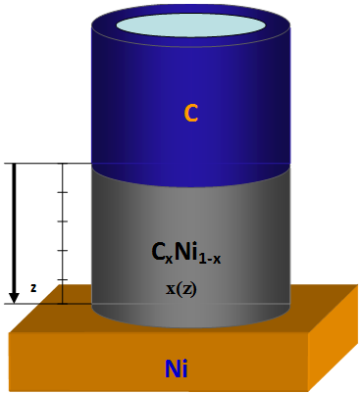

Figure 4. Model of CNT-Ni interconnect as a disordered alloy.

a pre-defined CNT geometry.

2. Multiple scattering theory and effective medium approach for CNT simulations

2.1. Electronic structure calculations

We consider the resistivity as a scattering problem, where the current carriers participate in the transport, according to various mechanisms based on the presence of scattering centers (phonons, charge defects, structural defects, *etc.*), including a pure elastic way called ballistic (Matissien rule). The scattering paradigm is presented in Fig. 5. The computational procedure developed by us for these calculations [5, 6] is based on the construction of the cluster potentials as well as the evaluation of the S- and T-matrices for scattering and transfer, respectively. This allows us to realize the full-scale electronic structure calculations for condensed matter ('black box'), where *influence* means a set of electronic 'trial' energy-dependent wave functions $\Psi_{in}(\mathbf{r})$ and *response* $\Psi_{out}(\mathbf{r})$ gives sets of scattering amplitudes corresponding to possible scattering channels for any 'trial' energy. This allows us to 'decrypt' the electronic spectra of 'black box'.

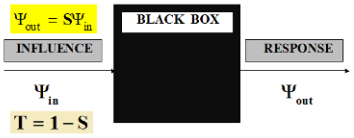

Figure 5. The scattering paradigm: Influence (*in*) and Response (*out*).

We consider a domain where the stationary solutions of the Schrödinger equation are known, and we label them by

$$\psi_{in}(\mathbf{r}) = \phi_{\mathbf{k}}(\mathbf{r}) = \exp(i\mathbf{kr}). \tag{1}$$

The scattering of 'trial' waves, in the presence of a potential, yields new stationary solutions labeled by

$$\psi_{out}(\mathbf{r}) = \psi_{\mathbf{k}}^{(\pm)}(\mathbf{r}) \tag{2}$$

for the modified Schrödinger equation

$$\hat{H}\psi_{\mathbf{k}}^{(\pm)}(\mathbf{r}) = E\psi_{\mathbf{k}}^{(\pm)}(\mathbf{r}).$$

An electronic structure calculation is considered here as a scattering problem, where the centers of scattering are identified with the atoms of clusters [5].
The first step of modeling is the construction of potentials, both atomic and crystalline. The Gaspar's potential (G) of screened atomic nucleus is defined as [9, 10]:

$$V_{coul}^{G}(r) = -\frac{2Z}{r}\frac{\exp\left(-\dfrac{\lambda r}{\mu}\right)}{\left(1+\dfrac{Ar}{\mu}\right)}, \tag{3}$$

where $\lambda = 0.1837, \mu = 0.8853Z^{-\frac{1}{3}}$ and $A = 1.05$. The electronic part of Gaspar's potential is $V_e(r) = \dfrac{2Z}{r} + V^G(r)$. Using a statistical approach for atoms, one usually applies X_α and $X_{\alpha\beta}$ presentations for the electronic exchange and correlation:

$$V_{X_\alpha}(\mathbf{r}) = -6\alpha\left(\frac{3\rho_e(\mathbf{r})}{8\pi}\right)^{\frac{1}{3}}, \tag{4}$$

where α depends on the charge number Z, and

$$V_{X_{\alpha\beta}}(\mathbf{r}) = \left[1 + \frac{\beta}{\alpha} G\left(\rho_e(\mathbf{r})\right)\right] V_{X\alpha}, \tag{5}$$

where

$$G(\rho_e) = \frac{4}{3}\left(\frac{\nabla\rho_e}{\rho_e}\right)^2 - 2\frac{\nabla^2}{\rho_e}\rho_e,$$

$\alpha = 0.67$ and $\beta = 0.003$, whereas the electron density function

$$\rho_e(\mathbf{r}) = \frac{\nabla_r V_e}{8\pi}.$$

Thus, the atomic potential of a neutral atom can be expressed as:

$$V_{at}(\mathbf{r}) = V_{coul}(\mathbf{r}) + V_{ex-corr}(\mathbf{r}), \tag{6}$$

where V_{coul} is the Gaspar's potential and $V_{ex-corr}$ is either V_{X_α} or $V_{X_{\alpha\beta}}$. Thus, both the crystalline potential and the electronic density function can be expressed using formulae:

$$V_{coul}(\mathbf{r}) = V^G_{coul}(r) + \sum_{\gamma,n_\gamma} V^G_{coul,\gamma}\left(\left|\mathbf{r} - \mathbf{R}^\gamma_{n_\gamma}\right|\right), \tag{7}$$

$$\rho_{e,cryst}(\mathbf{r}) = \rho_e(r) + \sum_{\gamma,n_\gamma} \rho_{e,\gamma}\left(\left|\mathbf{r} - \mathbf{R}^\gamma_{n_\gamma}\right|\right), \tag{8}$$

where summing is performed over the crystalline unit cell, γ defines a sort of atom while n_γ numerates positions of atoms separated by the corresponding R^γ_n interatomic distances. Fig. 6 shows both atomic and crystalline potentials for carbon as compared to the Hartree-Fock atomic potential.

Then, we apply the so-called muffin-tin approximation (*MTA*):

$$V_{MT}(\mathbf{r}) = \left\langle V_{cryst}(\mathbf{r})\right\rangle - V_{MTZ}, \tag{9}$$

where $V_{cryst}(\mathbf{r}) = V_{coul}(\mathbf{r}) + V_{ex-corr}(\mathbf{r})$, $V_{ex-corr}$ are the same potentials V_{X_α} or $V_{X_{\alpha\beta}}$ as in atomic case except for the electronic density, which is defined according to Eq. (8), whereas V_{MTZ} the *MT*-zero estimate of potential (so far, the most attention was paid to the spherical non-symmetrical *MT*-potentials).

To obtain the electronic structure, the calculations on scattering properties are necessary, generally, in the form of *S*- and *T*-matrices (Fig. 2). These calculations start with the definition of the initial atomic structure, to produce a medium for the solution of the scattering problem, for a trial electronic wave [5]. The results of potential modeling and phase shifts in the framework of the *MT*-approximation are presented elsewhere [5, 6].

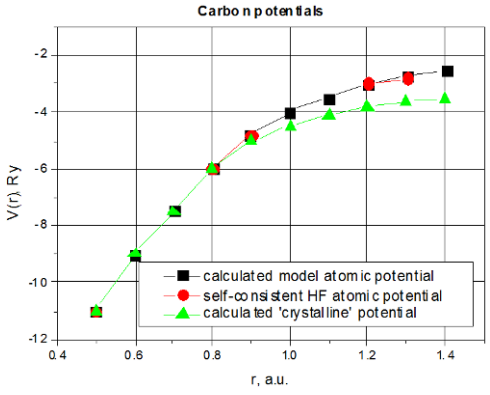

Figure 6. Analytical carbon potentials based on simulation procedure Eqs. (1-6) as compared to the results of Hartree-Fock calculations.

The formalism used by us for electronic structure calculations is based on the CPA approximation [7], the multiple scattering theory [11] and cluster approach [12]. As a *first step* in the modeling procedure, one postulates the atomic structure at the level of short- and medium-range orders. As a *second step* we construct a "crystalline" potential and introduce the muffin-tin (*MT*) approach. This is accomplished by using realistic analytical potential functions.

The scattering paradigm for the simplest cases of spherically symmetrical potential-scatterers (elastic scattering) looks as:

$$\psi(r) \to e^{ikz} + f(\theta)\frac{e^{ikr}}{r} \quad \text{("liquid metal" model case)} \tag{10}$$

and

$$\psi(\mathbf{r}) \to e^{ikz} + f(\theta,\varphi)\frac{e^{ikr}}{r} \quad \text{(spherical cluster model case).} \tag{11}$$

Then, the electronic wave scattering problem is solved: i) the energy dependence of the scattering properties for isolated *MT* scatterers is established, in the form of the phase shifts $\delta_{lm}(E)$, and ii) the *T*-matrix of the cluster is found as a whole.

In general, the modelling of disordered materials represents them as a set of atoms or clusters immersed in an effective medium, with the dispersion $E(\mathbf{K})$ and a complex energy-dependent coherent potential $\Sigma(E)$ found self-consistently in the framework of the CPA. The basic equations of this approach are:

$$\Sigma(E) = V_{eff} + \langle T\rangle\left(1 + G_{eff}\langle T\rangle\right)^{-1}, \tag{12}$$

$$G(E) = G_{eff} + G_{eff}\langle T\rangle G_{eff} = \langle G\rangle, \tag{13}$$

$$\langle T(E,\mathbf{K})\rangle = 0, \tag{14}$$

$$\Sigma(E) = V_{eff}, \tag{15}$$

$$\langle \mathrm{G}\rangle = \mathrm{G}(E) = \mathrm{G}_{eff}, \tag{16}$$

$$N(E) = -\frac{2}{\pi}\ln\{\det\|\mathrm{G}(E)\|\}. \tag{17}$$

Here $\langle\ldots\rangle$ denotes averaging, V_{eff} and G_{eff} are the potential and the Green's function of the effective medium, respectively, $T(E,\mathbf{K})$ the T matrix of the cluster, and $N(E)$ the integral density of the electronic states. Eq. (14) can be re-written in form:

$$\langle T(E,\mathbf{K})\rangle = \mathbf{Sp}T(E,\mathbf{K}) = \int_{\Omega_\mathbf{K}} \langle\mathbf{K}|T(E,\mathbf{K})|\mathbf{K}\rangle d\Omega_\mathbf{K} = 0, \tag{18}$$

where

$$|\mathbf{K}\rangle = 4\pi\sum_{l,m}(\mathrm{i})^l j_l(kr)Y^*_{lm}(\mathbf{K})Y_{lm}(\mathbf{r})$$

is the one-electron wave function, **Sp** means the calculation of the matrix trace while the integration is performed over all angles of $\mathbf{K}$ inside the volume Ω_K. The indices l and m arise, as a result of expansions of the functions as Bessel's functions j_l, Hankel's functions h_l and spherical harmonics Y_{lm}. Eq. (14) enables one to obtain the dispersion relation $E(\mathbf{K})$ of the effective medium. The DOS calculations have been performed according to the relation:

$$\rho(E) = \frac{\delta N(E)}{\delta E} = \frac{2}{\pi}\int \Im\{\mathbf{Sp}\mathrm{G}(\mathbf{r},\mathbf{r}',E)\}d\mathbf{r}, \tag{19}$$

where $\Im$ means the imaginary part of the matrix trace and

$$\mathrm{G}(\mathbf{r},\mathbf{r}',E) = \sum_{l,m} Y_{lm}(\mathbf{r})Y_{lm}(\mathbf{r}')\mathrm{G}_l(\mathbf{r},\mathbf{r}')$$

is the angular expansion of Green function.

The paradigm of scattering theory and the developed strategy of simulation of CNTs electronic properties uses the generalized scattering condition for the low-dimensional atomic structures of condensed matter (Quantum Scattering in d-Dimensions):

$$\psi^{(\pm)}_\mathbf{k}(\mathbf{r}) \underset{r\to\infty}{\propto} \phi_\mathbf{k}(\mathbf{r}) + f^{(\pm)}_\mathbf{k}(\Omega)\frac{\exp(\pm\mathrm{i}kr)}{r^{\frac{d-1}{2}}}, \tag{20}$$

where superscripts '+' and '-' label the asymptotic behavior in terms of d-dimensional waves:

$$\frac{\partial\sigma_{a\to b}}{\partial\Omega} = \frac{2\pi}{\hbar v}\left|\left\langle\phi_b\left|\hat{V}\right|\psi^+_a\right\rangle\right|^2\rho_d(E). \tag{21}$$

Following the scattering paradigm (see Eqs. (1), (2) and Fig. 5) we should take into account the dimension (see Eq. (20), $d = 2$) and symmetry of the scattering problem for nanotube modeling. This also means that the dispersion law of a scattered wave, Eq. (18), must be introduced as a sum of radial (r) and axial (z-axis) contributions, namely: $k^2 = k_r^2 + k_z^2$. These expansions are usually used for objects with cylindrical symmetry such as nanotubes [13–15]. In particular, the scattering model for a cylindrical atomic cluster allows us to calculate below the CNTs electronic structure for various diameters and chiralities.

2.2. Calculations of conductivity and resistance

The calculations of conductivity are usually performed using Kubo-Greenwood formula [16]:

$$\sigma_E(\omega) = \frac{\pi_\Omega}{4\omega}\int[f(E) - f(E+\hbar\omega)]|D_E|^2\rho(E)\rho(E+\hbar\omega)dE, \tag{22}$$

where ω is a real frequency parameter of Fourier transform for the time-dependent functions, $f(E)$ the Fermi-Dirac distribution function,

$$D_{E,E'} = \int_\Omega \Psi^*_{E'}\nabla\Psi_E d\mathbf{r},$$

$\Psi_{E(\mathbf{K})} = A\exp(\mathrm{i}\mathbf{K}\mathbf{r})$ and $\mathbf{K}$ is the complex wave vector of the effective medium. The dispersion function $E(\mathbf{K})$ determines the properties of the wave function $\Psi_{E(\mathbf{K})}$ upon the isoenergy surface in $\mathbf{K}$-space. The imaginary part of $\mathbf{K}$ ($\mathbf{K}_I$) causes a damping of the electron wave, due to the absence of the long-range structural order.

For static conductivity ($\omega = 0$ and $\mathrm{T} = 0$ K) Eq. (22) gives Drude-like formula:

$$\sigma_{E(K)} = \frac{e^2 n^*}{m^*}\tau, \tag{23}$$

where n^* is the effective electron density, with a relaxation time

$$\tau \approx \frac{l}{v_h},$$

$l(\mathrm{T})$ is the free path while a heat velocity is

$$v_h = \left(\frac{3k\mathrm{T}}{m^*}\right)^{\frac{1}{2}}.$$

The effective electron mass can be defined using the dispersion law:

$$m^* = \left(\frac{\partial^2 E}{\partial K_R^2}\right)^{-1}, \tag{24}$$

where K_R is a modulus of the real part of **K** vector.
Thus, there exist some ideas to estimate the conductivity in static and frequency regimes and to take into account temperature effects. However, in the case of CNT, we must consider not only the diffusive mechanism of conductivity, but also the 'so-called' ballistic one. This is an evident complication in the interpretation of electrical properties of CNTs and related systems.

3. 'Liquid metal' model for CNT-metal junction: *Ni-CNT case*

The term "liquid metal" means the structural disorder of the substance involved, more precisely, only the nearest order (short range order - SRO) is taken into account, as it usually occurs in a liquid. It also means that the interatomic distance from the nearest neighbor (first coordination sphere) is fixed, whereas the angular coordinates are random.
To implement this model, we focus the matter into a single atom (Fig. 7) which is associated with a crystalline potential in *MT*-approach, to consider the influence of the nearest vicinity. The neighbor atom around the studied atom is spread and, in fact, we are working on the one bond distance.

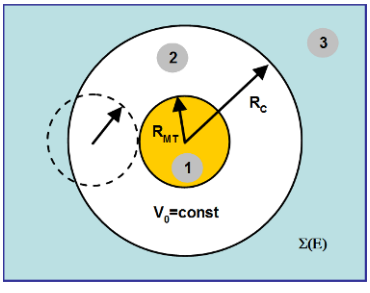

Figure 7. The "liquid metal" model.

The area 2 is a sphere of radius R_C determined from the condition of average matter density maintenance. However, to consider the influence of medium we need to "load" the sphere 2 with an effective complex potential, which defines the fading of electromagnetic waves, thereby modeling the disordered medium. The region 3 is under the influence of coherent potential $\Sigma(E)$. After that we must match the wave functions on the border of regions 2 and 3, superposing the Soven condition [17], which correspond to the statement that disordered media do not allow the forward scattering. The spherical symmetry of this system allows us to use partial decomposition techniques and the scattered wave outside the *MT*-sphere 2, where the potential is constant, defined as: $\psi_l^{(2)} = j_l(kr) - tg\delta_l n_l(kr)$. The next step is to find the dispersion law of the effective medium and the electronic density of states (EDOS). In "liquid" model, the argument **K** of dispersion function $E(\mathbf{K})$ is complex: $\mathbf{K}_R + i\mathbf{K}_I$. The CPA approach means:

$$\int_{\Omega_K} \langle \mathbf{K}|\tilde{t}\,|\mathbf{K}\rangle\, d\Omega_K = 0$$

(similar to Eqs. (14) and (18)).
Another condition is that the average density of matter is maintained also locally. For CNT-Ni junction (Figs. 3, 4), a 'liquid metal' model is calculated using the 'mixed' dispersion law [5, 17]:

$$E_{C-Ni}(\mathbf{K}_R) = xE_C(\mathbf{K}_R) + (1-x)E_{Ni}(\mathbf{K}_R). \qquad (25)$$

The metal alloy model is used for evaluation of mixed effective mass $m^*_{C-Ni}(E)$. Taking into account the spectral dependence of the effective mass $m^*(E)$ and estimating the spectral resistivity $\rho_x(E)$, we should estimate the average layer resistivity $\rho_{x,av}$ as:

$$\rho_{x,av} = \frac{\int_0^{E_{fin}} \rho_x(E)dE}{E_{fin}}, \qquad (26)$$

where E_{fin} is the estimated width of conduction band and $x(z)$ the stoichiometry coefficient depending on the coordinate z of ring layer (Fig. 4). An evaluation of resistance for the CNT-Ni contact gives $\sim$ 105 kOhm for the nanotube with the internal and external radii $R_1 = 1.0$ nm and $R_2 = 2.0$ nm. Evidently, the results of resistance evaluation for the interconnect depend essentially on both the layer height l_0 (C_xNi_{1-x} space, Fig. 4) and the spectral integration parameter E_{fin}, which is responsible for the electron transport of really activated electrons. The "liquid metal" model does not take into account CNT chirality in the interconnect space. Limitations on simulation of chirality effect (influence of chirality angle) in the CNT-Me junction forced us to develop the semi-empirical model which takes into account the local atomic structure of interconnect. For this aim, we have construct a model of 'effective bonds' for interconnect with the realistic atomic structure.

4. Simulation of CNT-Me interconnect: *'Effective bonds' model*

A model of the CNT-Me nanointerconnect [4] (Fig. 1) is developed in the current study. Within the electronic

transport formalism, it consists of two regions supporting the two different electron transport mechanisms: ballistic (elastic) and collisional (non-elastic). These electron transport processes are simulated by the corresponding boundary conditions in the form of the effective medium. The CNT chirality (*m*,*n*) is simulated by the corresponding orientation of carbon rings within the scattering medium (Fig. 8).

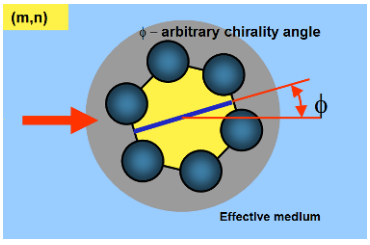

Figure 8. Modeling of chirality effects: carbon ring rotation within CNT.

The most problematic regions for simulation are CNT-Me junctions, where atomic structural disorder is observed and the conductivity mechanism is changed. The chirality influence on the resistance in the region of interconnect depends on the number of statistically realized bonds between the CNT and the catalytic substrate (*e.g.*, Ni, Cu, Au, Ag, Pd, Pt) formed during the CNT growth above the metallic catalyst surface.

4.1. Mechanism of the ballistic conductivity as a result of the multiple scattering

We assume that the conducting nanotubes are not very long and electrons are not drastically scattered by any defect (imperfection) of this nanomaterial. The effect of the charge accumulation is neglected as well. We are dealing with the so called 'ballistic' mechanism of the electronic transport. Such a model is similar to ideal billiards with moving elastic balls-electrons. This means that we consider that the length of CNT provides the ideal ballistic conductivity in conditions of standing waves in open resonator. According to the Landauer model [18],

$$g_{mn} = \frac{e^2}{h}\mathbf{Sp}(T_{mn}T_{mn}^{+}), m \neq n,$$

where g_{mn} are the conductance coefficients while $\frac{e^2}{h}T_{12}\Delta\mu$ is the current flow between the two reservoirs with a difference between the chemical potentials $\Delta\mu = \mu_1 - \mu_2$ (T_{12} is the transmission coefficient found to be between 1 to 2 in the one-channel case) based on the conception of the quantum conductance $\frac{2e^2}{h} = 0.077$ kOhm^{-1} (or, the resistance is about 12.92 kOhm).

Using the simulation models, presented earlier [5], we have developed resistance models for both SW and MW CNT-Me interconnects, based on the interface potential barriers evaluation and Landauer formula, which defines the integrated conductance:

$$I_G = \frac{2e^2}{h}\sum_{i=1}^{N} T_i = \left(\frac{1}{12.92(k\Omega)}\right)\sum_{i=1}^{N} T_i = 0.0774\sum_{i=1}^{N} T_i, \quad (27)$$

where N is the number of conducting channels and T_i the corresponding transmission coefficient.

4.2. Chirality and thickness simulations

Fig. 9 presents a simulation of catalytic growth of CNT upon the metal substrate. This is accompanied by creation of C-Me 'effective bonds'. We consider here the (001) substrates of some *fcc*-metals. We should also point out that this is a probabilistic process when only more-or-less equilibrium bonds ("effective bonds") are formed at inter-atomic distances corresponding to the minimum total energies. The evaluation of a number of "effective bonds" using Eq. (27) is principal for the number of "conducting channels", since the conductance is proportional to the number of apparent "effective bonds" within the CNT-Me interconnect.

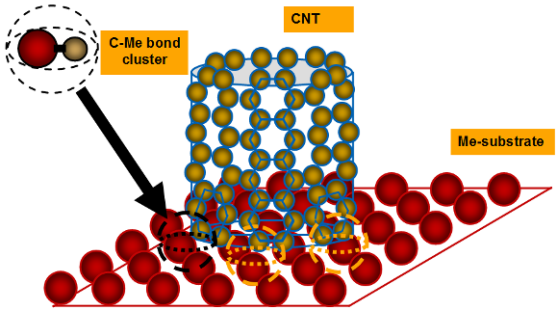

Figure 9. The SW CNT-Me interconnect: model of "*effective bonds*".

The calculation of conducting abilities of "effective bond" leads us to estimate the energy-dependent transparency coefficient of a potential barrier C-Me (Fig. 10), which belongs to scattering problems. The scattering process for a C-Me potential barrier is also regulated by the effect of "thin film" for conductivity electrons, which leads to quantization in voltaic parameters (in the case of full transparency). The transmission (transparency) coefficient

T for the barrier scattering problem (Eq. (28) and Fig. 10) is defined as:

$$T = \sqrt{\frac{E_2}{E_1}} \left(\frac{2\sqrt{E_1}}{\sqrt{E_1} + \sqrt{E_2}} \right)^2, \qquad (28)$$

where E_1 and E_2 are the corresponding electron energies. Evaluation of resistances R_i for CNT-Ni junctions for various nanotube diameters and chiralities are present in Table 1 (see also Figs. 9 and 10).

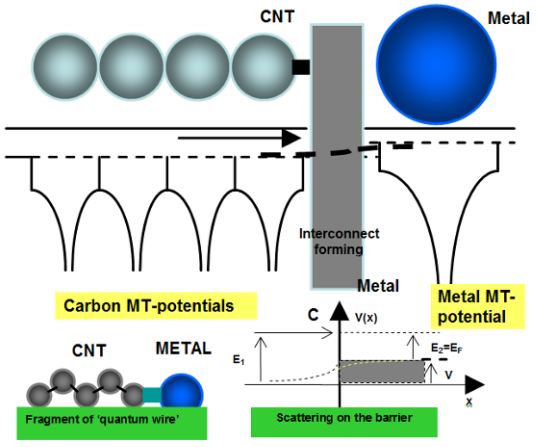

Figure 10. The formation of potential barrier for SW CNT-Me interconnect.

These resistances have been estimated taking into account that only thermally activated electrons (i.e., a small part of all electrons) take a part in the conduction process with Fermi velocity v_F. This ratio can be estimated as:

$$\frac{\Delta n}{n} \approx \frac{3}{4} \frac{kT}{E_F}, \qquad (29)$$

where n is the quasi-free electron concentration, for T = 300 K, $kT = 0.0258$ eV.

The role of thermally activated electron is described by the scattering mechanism changing in the space of CNT-Me interconnect. The mean free path L in the CNT is of order $10^2 - 10^4$ a_C, where a_C is a carbon covalent radius, which can be explained by the ballistic mechanism of electron transport within the energy channel of the CNT. In the vicinity of the interconnect, we observe a drastic decrease of the electron mean free path down to 1-2 a_C. From the uncertainty condition $\kappa L \approx 1$ (where $L \sim a_C \sim 2a.u.$ is a free path), we can evaluate the Fermi electron wave number $\kappa \propto \kappa_F \approx \frac{1}{a_C} \approx 0.5 a.u.^{-1}$. It means that $E_F \sim 0.25$

Table 1. Simulation of resistance for the SW CNT-Ni interconnect (Fig. 9).

Diameter, nm	Chirality indices (Fig. 8)	Number of bonds in contact	Modulus of chirality vector, nm	Interconnect resistance, kOhm
zig-zag, $\varphi = 0°$				
1.010	C(13,0)	12	2.952	665.19
2.036	C(26,0)	24	6.394	333.33
5.092	C(65,0)	64	15.990	124.72
10.100	C(130,0)	129	32.002	61.87
20.360	C(260,0)	259	63.940	30.82
armchair, $\varphi = 30°$				
0.949	C(7,7)	12	2.982	665.19
2.035	C(15,15)	28	6.391	205.71
5.021	C(37,37)	72	15.765	111.11
10.041	C(74,74)	146	31.531	54.79
20.084	C(128,128)	294	63.062	27.21
C(3*m*,*m*), $\varphi = 14°$				
0.847	C(9,3)	3	2.66	2666.66
1.694	C(18,6)	5	5.32	1600.00
5.082	C(54,18)	16	15.96	500.00
10.16	C(108,36)	36	32.05	222.22
20.32	C(216,72)	80	64.10	100.00
C(2*m*,*m*), $\varphi = 19°$				
1.036	C(10,5)	5	3.254	1600.00
2.072	C(20,10)	9	6.508	888.88
4.973	C(48,24)	17	15.614	470.50
10.1528	C(98,49)	47	31.880	170.21
20.5128	C(198,99)	97	64.410	82.47

Ry, i.e., a large increase of resistance occurs in the interconnect space. In particular, the variation of the chirality angle ϕ within the interconnect space leads to a fluctuation of the number of C-Me atomic bonds. In the case of $0° < \phi < 30°$, a certain number of non-stable and non-equilibrium bonds can be created. Evidently, this leads to a decrease of interconnect conductance, which is well-observed when performing variation of nanotube diameter (Fig. 11):

Specific results for chirality effect simulations are shown in Fig. 12, with an evident maximum of the resistance for $\phi \approx 15°$, where the large number of non-equilibrium bonds is formed, with higher potential barriers and lower transparency.

Fig. 13 shows the generalized results of simulations on resistance of junctions obtained for various metallic substrates. It is clear that Ag and Au substrates are more effective electrically while Ni is rather a 'worse' substrate for interconnect, although it yields the most effective catalyst for CNT growth. On the other hand, the catalysts which are usually used for the SW CNT growth (*e.g.*, Fe, Co and Ni), have a stronger bound to the ends of SW CNTs than noble metals [19], *i.e.*, some compromise ex-

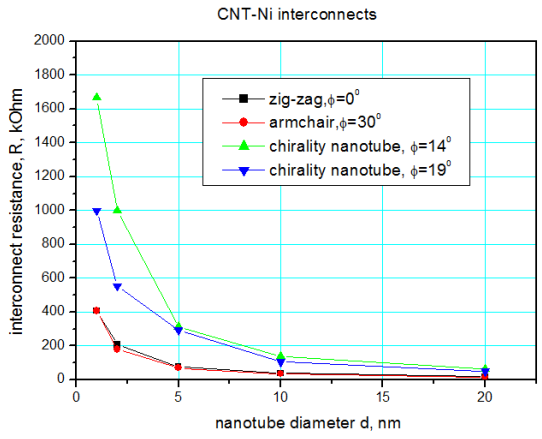

Figure 11. CNT-Ni interconnect resistance *via* NT diameter.

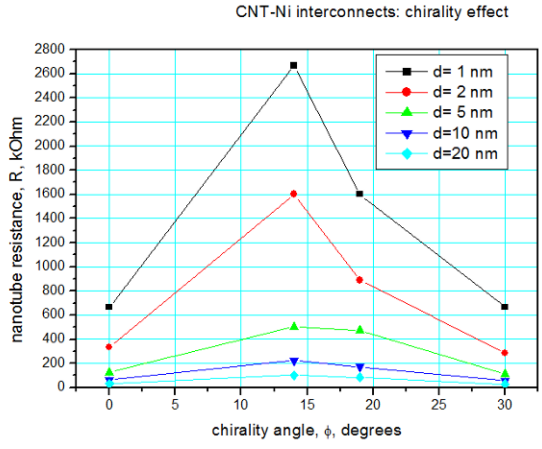

Figure 12. CNT-Ni interconnect simulation: *chirality effects*.

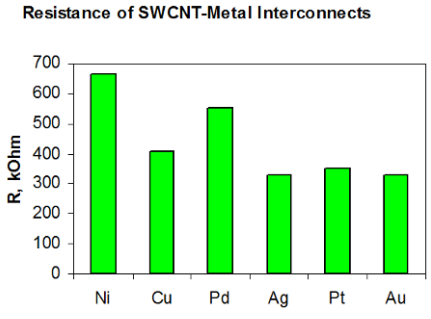

Figure 13. Resistances of the zigzag-type SW CNT-Me interconnects for the CNT diameter ~ 1 nm.

ists between electrical parameters and strengths of the interconnect bonding.

5. Simulations on MW CNT-Me interconnects: conductance and resistance

Our current study focuses on the development of models describing the growth mechanism of carbon nanotubes upon nanostructured Ni catalyst inside the pores of Al_2O_3 membranes. The scope of these simulations allows us to predict that a specific morphology of CNTs could be formed inside the specific membranes having defined periodicity and hole dimensions. These simulations are necessary, in order to understand the basic mechanism of CNT growth and to achieve the tight control on the fabrication process. We have constructed atomistic models of both SW CNT bundles and MW CNTs which could fit into a porous alumina with holes diameters ~20-21 nm. In particular, a multi-shell model of MW CNT is presented in Fig. 14, with a pre-defined combination of *armchair* (*ac*) and *zig-zag* (*zz*) shells (Table 2).

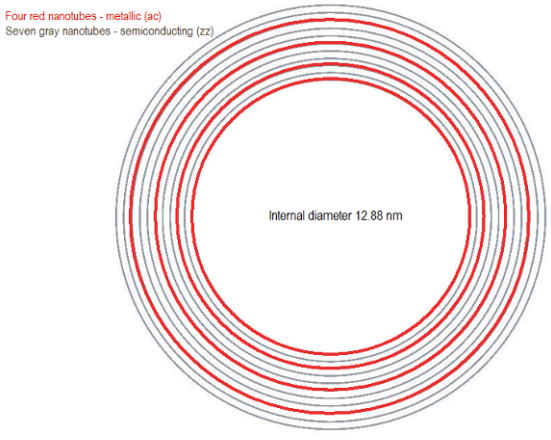

Figure 14. A cross-section of the supercell model for MW CNT with height 6.39 nm and external diameter 19.89 nm.

Using the simulation models presented earlier, we have developed an "effective bonds" model for MWCNT-Me junction resistance [20] based on the interface potential barriers evaluation and Landauer formula, Eq. (27). Results of these simulations are presented in Figure 15 and Table 3. Again, Fig. 15 shows similar ratios of electric resistances as for SW CNTs (Fig. 13), in favor of Au, Ag and Pd.

However, in the case of MWCNT-Me junction, the integral

Table 2. Details of the model for MW CNT-Me interconnect.

Diameter of CNT shell, nm	Chirality
12.88	(95,95) *ac*
13.54	(173,0) *zz*
14.24	(105,105) *ac*
14.87	(190,0) *zz*
15.58	(199,0) *zz*
16.27	(120,120) *ac*
16.99	(217,0) *zz*
17.69	(226,0) *zz*
18.44	(136,136) *ac*
19.18	(245,0) *zz*
19.88	(254,0) *zz*

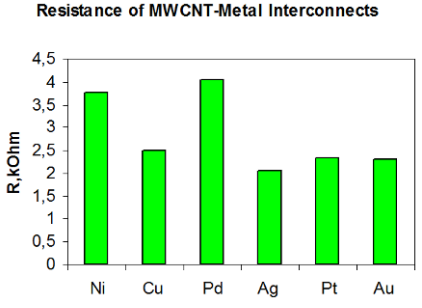

Figure 15. Resistances of various MWCNT-Me interconnects.

Table 3. Simulation of resistances for the MW CNT-Me interconnects.

Metal	Z	Interconnect resistivity, kOhm
Au	79	2.313
Pt	78	2.345
Pd	47	4.050
Ag	46	2.062
Cu	29	2.509
Ni	28	3.772

mechanical bonding with a corresponding substrate may be not so significant as in the case of SW CNTs, where the weak bonding can be principal.

6. Evaluation of current loss between the adjacent shells inside the MW CNT

Using the model of inter-shell potential within the MW CNT we also have evaluated the transparency coefficient, which determines the possible 'radial current' losses. Fig. 16 shows the inter-shell potential which is calculated using the developed realistic analytical potentials (see comments in Section 2 and the procedure of the potential construction, *e.g.*, in [3]).

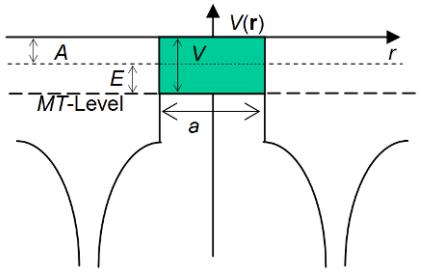

Figure 16. Inter-shell transparency and inter-shell *MT*-potential model (*MT*-muffin tin).

In Fig. 16, A is the electron emission energy, E the electron energy, V the height of the potential barrier between the nearest atoms in neighboring nanotube shells. Thus, a radial transparency coefficient T for the two different energy ratios can be defined as:

$$E > V, T = \frac{4Ek_2^2}{\left(E - k_2^2\right)\sin^2 k_2 a + 4Ek_2^2}, k_2^2 = E - V, \quad (30)$$

$$E < V, T = \frac{4E\kappa_2^2}{\left(E - \kappa_2^2\right)sh^2\kappa_2 a + 4E\kappa_2^2}, \kappa_2^2 = V - E, \quad (31)$$

where k_2 the electron wave number in the case of above-barrier motion and κ_2 the same for under-barrier motion. For example, between the 2nd and 1st shells (*zz*-*ac* case, Fig. 14) $a = 13.54 - 12.88 = 0.66$ nm $= 12.47$ a.u. and $T = 3.469 \cdot 10^{-6}$ *per* 1 bond.

The total radial conductance is proportional to both T and the number of effective potential barriers. It is also clear that the 'radial current' losses (or, simply radial current) are similar to the Hall current due to the induced magnetic field of the basic axial current. A pure scattering mechanism is also possible. However, the radial conductance *per* CNT length depends on the morphology (chirality) of the nearest nanotubes, when the number of shortest effective barriers is varied in a probabilistic way. This also

means that current-voltage parameters of MW CNTs can be less stable, than in the case of SW CNTs. It was found that inter-shell interactions, such as inter-shell tunneling of electrons and Coulomb interactions [21–23] cause a reduction of the total MW CNT conductance.

7. Conclusions

Using the *'effective bonds'* model, we have predicted the resistivity of interconnects between the metal substrate (*e.g.*, Ni) and the SW or MW CNTs. There also exists a qualitative compatibility of results obtained for the CNT-Me junctions using both approaches considered in this paper: (*i*) first principles *'liquid metal'* model and (*ii*) semi-empirical *'effective bonds'* model based on the Landauer relationship. At the same time, the latter results are quantitatively comparable with those measured experimentally, *i.e.*, within the range from several up to 50 kOhm [24].

We have also developed the model of inter-shell interaction for the MW CNTs, which allows us to estimate the transparency coefficient as an indicator of possible 'radial current' losses. We have underscored that a conductance and other current-voltaic parameters depend on the morphology of the nearest shells in MW CNTs, which leads to complications for technology and production of nanodevices with the stable electric characteristics.

Acknowledgments

This study has been supported by grant EC FP7 ICT-2007-1, Proposal for 21625 CATHERINE Project (2008-2010): *C*arbon n*A*notube *T*echnology for *H*igh-speed n*E*xt-gene*R*ation nano-*I*nterconn*E*cts. We thank Prof. E.A. Kotomin for stimulating discussions.

References

[1] M. Ahlskog, Ch. Laurent, M. Baxendale, M. Huhtala, In: H.S. Nalwa (Ed.), Encyclopedia of Nanoscience and Nanotechnology, Vol. 3 (American Sci. Publishers, Valencia, CA, 2004) 139

[2] M.S. Dresselhaus, G. Dresselhaus, P.C. Eklund, Science of Fullerenes and Carbon Nanotubes (Academic, San Diego, 1996)

[3] S.J. Tans, R.M. Verschueren, C. Dekker, Nature 393, 49 (1998)

[4] J. Tersoff, Appl. Phys. Lett. 74, 2122 (1999)

[5] Yu.N. Shunin, K.K. Schwartz, In: R.C. Tennyson, A.E. Kiv (Eds.), Computer Modelling of Electronic and Atomic Processes in Solids (Kluwer Acad. Publisher, Dodrecht, Boston, London, 1997) 241

[6] Yu.N. Shunin, DSc Habil. thesis, University of Latvia (Riga-Salaspils, Latvia, 1991)

[7] E.L. Economou, Green's Functions in Quantum Physics, 3rd edition, Solid State Ser. Vol. 7 (Springer Verlag, Berlin, Heidelberg, 2006)

[8] J.M. Ziman, Models of Disorder (Cambridge Univ. Press, London, New York, 1979)

[9] R. Gaspar, Acta Phys. Acad. Sci. Hung. 2, 15 (1952)

[10] R. Gaspar, Acta Phys. Acad. Sci. Hung. 3, 263 (1954)

[11] J.C. Slater, The Self-Consistent Field for Molecules and Solids, Vol.4 (McGraw-Hill Book Company, New York, 1974)

[12] H. Ehrenreich, L. Schwartz, The Electronic Structure of Alloys, Solid State Phys. Vol. 31 (Academic Press, New York, San Francisco, London, 1976)

[13] M.F. Lin, K.W.-K. Shung, Phys. Rev. B 47, 6617 (1993)

[14] G. Gumbs, G.R. Aizin, Phys. Rev. B 65, 195407 (2002)

[15] G. Gumbs, A. Balassis, Phys. Rev. B 71, 235410 (2005)

[16] Yu.N. Shunin, Yu.F. Zhukovskii, S. Bellucci, Computer Modelling and New Technologies 12(2), 66 (2008)

[17] P. Soven, Phys. Rev. 156, 809 (1967)

[18] D. Stone, A. Szafer, IBM J. Res. Dev. 32, 384 (1988)

[19] F. Ding et al., Nano Lett. 8, 463 (2008)

[20] Yu.N. Shunin, In: H. Dosch, M.H. Van de Voorde (Eds.), GENNESYS White Paper (Max-Planck-Institut für Metallforschung, Stuttgart, 2009) 8

[21] S. Uryu, Phys. Rev. B 69, 075402 (2004)

[22] A.M. Lunde, K. Flensberg, A.-P. Jauho, Phys. Rev. B 71, 125408 (2005)

[23] Z. Kordrostami, M.H. Sheikhi, R. Mohammadzadegan, Fuller. Nanotub. Car. N. 16, 66 (2008)

[24] J.-O. Lee, J. Phys. D: Appl. Phys. 33, 1953 (2000)